Toxicology Letters 207 (2011) 258–269

Contents lists available at SciVerse ScienceDirect

Toxicology Letters

journal homepage: www.elsevier.com/locate/toxlet

Water-soluble germanium nanoparticles cause necrotic cell death and the damage can be attenuated by blocking the transduction of necrotic signaling pathway

Yu-Hsin Ma[a], Chin-Ping Huang[b], Jia-Shiuan Tsai[a], Mo-Yuan Shen[b], Yaw-Kuen Li[b,**], Lih-Yuan Lin[a,*]

[a] Institute of Molecular and Cellular Biology, and Department of Life Science, National Tsing Hua University, Hsinchu, Taiwan
[b] Department of Applied Chemistry, National Chao-Tung University, Hsinchu, Taiwan

ARTICLE INFO

Article history:
Received 25 May 2011
Received in revised form
20 September 2011
Accepted 21 September 2011
Available online 29 September 2011

Keywords:
Water-soluble germanium nanoparticles
Cytotoxicity
Calcium
Reactive oxygen species
Mitochondrial membrane potential
Necrosis

ABSTRACT

Water-soluble germanium nanoparticles (wsGeNPs) with allyamine-conjugated surfaces were fabricated and emit blue fluorescence under ultraviolet light. The wsGeNP was physically and chemically stable at various experimental conditions. Cytotoxicity of the fabricated wsGeNP was examined. MTT assay demonstrated that wsGeNP possessed high toxicity to cells and clonogenic survival assay further indicated that this effect was not resulted from retarding cell growth. Flow cytometric analysis indicated that wsGeNP did not alter the cell cycle profile but the sub-G1 fraction was absent from treated cells. Results from DNA fragmentation and propidium iodide exclusion assays also suggested that apoptotic cell death did not occur in cells treated with wsGeNP. Addition of a necrosis inhibitor, necrostatin-1, attenuated cell damage and indicated that wsGeNP caused necrotic cell death. Cell signaling leads to necrotic death was investigated. Intracellular calcium and reactive oxygen species (ROS) levels were increased upon wsGeNP treatment. These effects can be abrogated by BAPTA-AM and N-acetyl cysteine respectively, resulting in a reduction in cell damage. In addition, wsGeNP caused a decrease in mitochondrial membrane potential (MMP) which could be recovered by cyclosporine A. The cellular signaling events revealed that wsGeNP increase the cellular calcium level which enhances the production of ROS and leads to a reduction of MMP, consequentially results in necrotic cell death.

1. Introduction

Germanium (Ge) is a metalloid with semiconductor property and is dispensable for human health. Inorganic Ge compound, such as GeO_2, is generally non-toxic although renal and neural damages are reported after long-term, high-dose consumption. However, organic Ge compound, such as Ge-132, is regarded as an elixir in several countries since Ge-132 has been shown to inhibit cancer development (Kumano et al., 1985), induce erythropoietic efficiency (Dozono et al., 1996), exert antimicrobial activity (Aso et al., 1989) or modulate immunopotency (Fukazawa et al., 1994). We have shown that GeO_2 blocks cell cycle progression at G2 phase and causes radiosensitizing effect despite the chemical itself is very low in cytotoxicity (Chiu et al., 2002). High concentration of GeO_2 is required to generate the radiosensitizing effect. However, GeO_2 has a low solubility which hinders its biological application. In addition, GeO_2 cannot be delivered to a specific target to exert its radiosensitizing effect. Alternatively, nano-sized germanium particles may be utilized for this purpose.

Quantum dots (QDs) are generally defined as nanometer-sized crystals fabricated from materials with semiconductor properties. Due to their unique physical properties, QDs are currently utilized in various photoelectronic and biomedical researches. Materials with direct bandgap, such as CdSe, CdSe/ZnS, InP and PbSe, have photonic property under defined particle size (Alivisatos, 2004; Michalet et al., 2005). Semiconductor materials (Group IV) with indirect bandgap, i.e., Si(0) or Ge(0) are rarely characterized since they do not emit photons or fluoresce effectively at infrared region (Warner and Tilley, 2006; Zhou et al., 2003). However, germanium nanoparticles (GeNP) with sizes lower than the relatively large excitation Bohr radius (R_b = 11.5 nm) exert direct bandgap and produce radiative recombination. Hence GeNP fluoresces at the visible region. Due to quantum confinement and narrow size distribution, GeNPs were also defined as quantum dots(Kauzlarich et al., 2004; Warner and Tilley, 2006).

With a semiconductor property, Ge or Ge compounds are widely used in industries. It has been applied to fiber-optic systems, infrared optics, polymerization catalyst, various electronic devices and solar cells (Bailey et al., 2002; Rieke, 2007; Thiele, 2001;

* Corresponding author. Tel.: +886 3 5742693.
** Corresponding author.
E-mail address: lylin@life.nthu.edu.tw (L.-Y. Lin).

0378-4274/$ – see front matter © 2011 Elsevier Ireland Ltd. All rights reserved.
doi:10.1016/j.toxlet.2011.09.018

Washio, 2003). With the development of nanotechnology, nano-sized particles of Ge or Ge compounds have been fabricated. Owing to the distinct physical and optical properties, GeNP can potentially be used in a variety of fields (Chiu et al., 2006; Singh et al., 2005; Xie et al., 2009).

Fabrications of GeNP have been described using physical and chemical approaches. Physically, GeNP can be constructed with reactive laser ablation (Riabinina et al., 2006) or pulse laser with ion implantation (Ngiam et al., 1994). Chemically, several methods employing high temperatures and high reducing environment have been reported (Chiu and Kauzlarich, 2006; Fok et al., 2004; Lu et al., 2005). The drastic reaction conditions complicated the concoction procedures. Furthermore, it is difficult to control the size of the fabricated particles or modify the particle surfaces. The vapor condensation method (Warner and Tilley, 2006) for the manufacturing of GeNP is easy to follow and without the high temperature or reducing environment. Nonetheless, the prepared particles aggregated in aquatic phase and difficult to use in biological research (Lin et al., 2009). Recently, the method of synthesizing water-soluble GeNP (wsGeNP) has been reported and it potentially avoided the defects of previous methods (Lambert et al., 2007). GeNP produced by vapor condensation method has less toxicity to cells (Lin et al., 2009). The toxicity of GeNP fabricated through other methods has not been investigated.

With the synthesis of wsGeNP, the surface chemistry can be modified. The modifications may be useful for potential biological applications, such as cell type specific targeting. Since we have demonstrated that GeO_2 and GeNP are radiosensitizers in Chinese hamster ovary (CHO) K1 cells, we examined whether wsGeNP had the same property. We therefore prepared wsGeNP for cellular studies. The cytotoxicity of the wsGeNP was examined. Different from that of GeO_2 and GeNP, the wsGeNP damages cells at low concentration. The toxicological mechanism was studied and chemicals that attenuate the toxicity were signified.

2. Materials and methods

2.1. Cell culture and chemicals

CHO K1 cells were cultured as monolayers at 37 °C in McCoy's 5A medium supplemented with 10% heat-inactivated fetal bovine serum, 0.22% sodium bicarbonate, 100 U/ml ampicillin and 100 μg/ml streptomycin, in 5% CO_2/95% air and 100% humidity. Reagents for cell culture were purchased from GIBCO (Invitrogen). BAPTA-AM [1,2-bis-(o-aminophenoxy)-ethane-N,N,N′,N′-tetraacetic acid, tetraacetoxymethyl ester] was obtained from BIOMOL. Necrostatin-1 [5-(indol-3-ylmethyl)-(2-thio-3-methyl)hydantoin] was obtained from Merck. Cyclosporin A and Fluo-3/AM (1-[2-amino-5-(2,7-dichloro-6-hydroxy-3-oxo-3H-xanthen-9-yl)]-2-(2′-amino-5′-methylphenoxy)ethane-N,N,N′,N′-tetraacetic acid pentaacetoxymethyl ester) were acquired from Kelowna. $DiOC_6$ [3,3′-dihexloxa-carbocyanine iodide] was a product of Calbiochem. MTT [3-(4,5-dimethylthiazol-2-yl-2, 5-diphenyl tetrazolium bromide)] was purchased from USB Crop. ATPLite 300 assay kit was a product of Blossom. Other chemicals were purchased from Sigma unless specified.

2.2. Fabrication of wsGeNP

GeNP was synthesized in reverse micelles by reducing the solution-phase $GeCl_4$ (Warner and Tilley, 2006). All reactions were processed under a nitrogen atmosphere to slow down the oxidation of germanium. The reverse micelles solution was prepared by stirring 100 μl of $GeCl_4$ (1.0 M, anhydride) and 1.5 g of tetraoctylammonium bromide (TOAB) in 100 ml of anhydrous toluene for 30 min. GeNP were formed by rapidly adding 2 ml of the reducing agent (1 M lithium triethylborohydride [$Li(C_2H_5)_3BH$] in tetrahydrofuran) to the reverse micelles solution, which turned from clear to a translucent yellow color. The solution was left to react for a further 2 h then quenched with 20 ml of anhydrous methanol. In order to add amino groups onto the GeNP surface, 40 μl of a platinum catalyst (0.05 M H_2PtCl_6 in isopropyl alcohol) and 10 ml of allyamine were mixed with the GeNP solution and stirred for 30 min. After surface capping, the mixture was removed from the nitrogen environment and dried in a rotary evaporator, leaving behind the TOAB (white powder) and the GeNP. The allyamine capped GeNP was solubilized with 50 ml of distilled water and the TOAB was removed by filtration through a 0.22 μm filter. The product was designated as wsGeNP.

2.3. Fourier transfer infra red (FTIR) spectrophotometric analysis

Allyamine or allyamine-coated GeNP was mixed with oven-dried FTIR grade KBr to a final concentration of 1% (w/w). The mixture was grounded to a fine powder then flattened into thin films under 10 tons in a hydraulic press for FTIR measurements. FTIR spectra were obtained with a Nicolet Avatar 320 FTIR spectrometer (Nicolet. Instrument Co., Madison, WI, USA). Thirty two scans were collected at a spectral resolution of 1 cm^{-1}.

2.4. MTT assay

The cytotoxicity of the synthesized wsGeNP was evaluated using MTT assay. Briefly, CHO K1 cells were seeded in 96-well plates at a density of 3.5×10^3 cells/well and treated with various concentrations of wsGeNP at 37 °C for 24 h. Cells were then incubated with MTT (final concentration 0.4 mg/ml) for 4 h before harvesting. Cells were washed with phosphate-buffered saline (PBS) and 200 μl DMSO was added to each well. The absorbance of formazan was recorded at 565 nm with a ThermoMax microplate reader (Molecular Devices, Sunnyvale, CA, USA).

2.5. Clonogenic survival assay

Two hundred and fifty cells were seeded in 60 mm dish before treating with various concentrations of wsGeNP for 24 h. The wsGeNP was removed and cells were cultured in fresh medium for 7 days, then fixed and stained with 1% (w/v) crystal violet dissolved in 30% ethanol. Colonies containing at least 50 cells were counted. The survival fraction of each treatment was determined by dividing the number of colonies in the treated sample by that of the non-treated control sample.

2.6. Cell cycle analysis

Cells were treated with various concentrations of wsGeNP for 24 h. Treated cells were removed by trypsinization and collected by centrifugation at 1500 rpm for 10 min. The cell pellets were resuspended in 70% ethanol and stored at 4 °C overnight. Cells were then centrifuged and resuspended in 1 ml PBS containing RNase A (100 μg/ml). After 30 min at room temperature, the cells were spun down and the pellets stained with 1 ml of propidium iodide (PI, 20 μg/ml in PBS) for 30 min. Flow cytometric analysis was then carried out on a FACScalibur (Becton Dickinson, Franklin Lakes, NJ, USA).

2.7. DNA fragmentation assay

For DNA ladder analysis, cells were treated with 5 μM wsGeNP or irradiated with 25 J/m^2 UV. After further incubating at 37 °C for 24 h, cells were washed twice with PBS and the low-molecular-weighted DNA fragments were extracted with TTE buffer (0.2% Triton X-100, 10 mM Tris, 15 mM EDTA, pH 7.6) for 15 min at room temperature. After centrifuging at 12,000 rpm for 15 min, the supernatants were transferred to new tubes before RNAase A (100 μg/ml) was added and incubated at 37 °C for 1 h. DNA was extracted with 1 volume of phenol/chloroform/isoamyl alcohol and precipitated in 0.1 volume of 3 M sodium acetate (pH 5.2) and 1 volume of isopropyl alcohol. After standing at −70 °C for 15 min, the DNA was spun down at 12,000 rpm for 20 min, and washed with 70% alcohol. The DNA pellet was dissolved in TE buffer and analyzed electrophoretically on a 2% agarose gel.

2.8. Caspase-3 activity assay

Cells were lysed in 1% Triton X-100, 1% NP-40, 2 μg/ml aprotinin, 2 μg/ml leupeptin, 2 mM PMSF and incubated on ice for 10 min. After centrifugation at 13,000 rpm and 4 °C for 30 min, the supernatants were transferred to new tubes. Protein concentrations were determined using a protein assay kit (Bio-Rad). 50 μg of proteins were incubated at 37 °C in 100 μl reaction buffer (10 mM HEPES, 2 mM EDTA, 10 mM KCl, 1.5 mM $MgCl_2$, 10 mM DTT) containing 50 μM Ac-DEVD-AFC for 1 h. The AFC fluorescence was measured at excitation wavelength of 405 nm and emission wavelength of 505 nm with a microplate reader (Wallac 1420 Multilabel Counter, Perkin Elmer).

2.9. PI exclusion assay

The integrity of plasma membrane was assessed by determining the ability of cells to exclude PI. Cells were trypsinized, collected by centrifugation, washed once with PBS then suspended in PBS containing 10 μg/ml PI. The cells were stood at room temperature in the dark for 15 min. The levels of PI incorporation were determined by flow cytometry (FACScalibur, Becton Dickinson, Franklin Lakes, NJ, USA). The proportion of cells stained with PI was expressed as percentage of PI uptake.

2.10. Determination of intracellular Ca^{2+}, reactive oxygen species (ROS) and mitochondrial membrane potential (MMP)

Intracellular Ca^{2+}, ROS and MMP were measured by Fluo-3-AM, H_2DCF-DA and $DiOC_6$, respectively. Cells were treated with various concentrations of wsGeNP in the

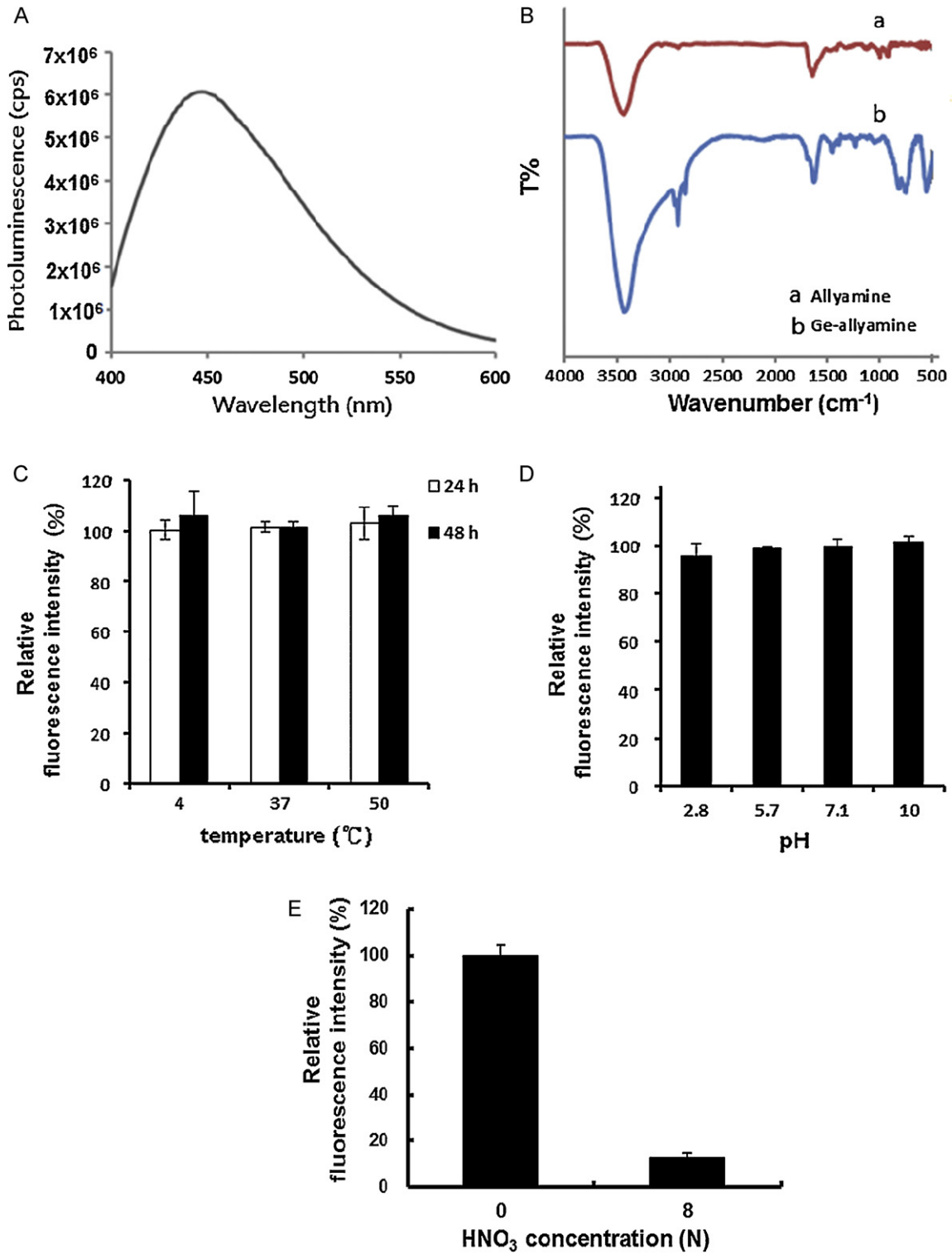

Fig. 1. Characterization of the synthetic wsGeNP. (A) The fluorescence emitted by the fabricated wsGeNP was analyzed with excitation and emission wavelengths of 350 and 450 nm, respectively. (B) The FTIR spectrum of the wsGeNP was analyzed to show the presence of allyamine on the surface of the particles. (C) Equivalent concentration (0.1 nM) of wsGeNP was incubated at different temperatures for 24 or 48 h and fluorescence intensity was compared with that without incubation. (D) Equivalent concentration (0.1 nM) of wsGeNP was incubated at different pH for 24 h at room temperature. Fluorescence intensity was determined after the incubation and compared with that of the sample without incubation. (E) Equivalent concentration (0.5 nM) of wsGeNP was dissolved in 8 N HNO_3 and the intensity of the fluorescence was determined. Each value represents a mean ± standard deviation of three samples.

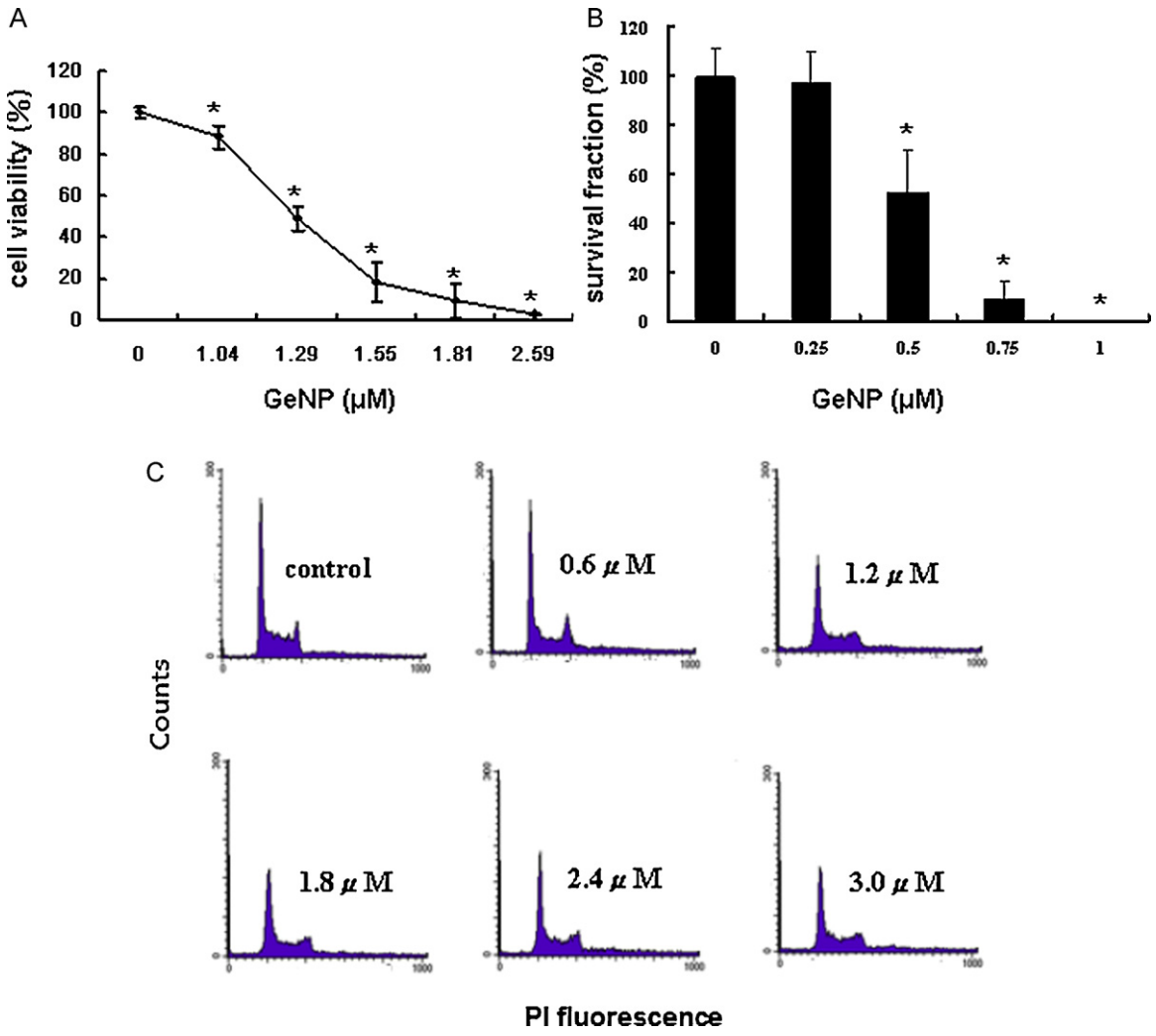

Fig. 2. Analysis of cell viability and cell cycle distribution after wsGeNP treatment. Cells were treated with various concentrations of wsGeNP for 24 h and cell viability was examined by MTT (A) and clonogenic survival (B) assay. Cell population distributed in the cell cycle was determined by flow cytometry (C). Each value represents a mean ± standard deviation of three samples. *Significant difference ($p < 0.05$).

presence or absence of inhibitors for the indicated time intervals. Two μM Fluo-3-AM, 5 μM H_2DCF-DA or 40 nM $DiCO_6$ was added 30 min before cell harvest. Cellular fluorescence was measured using flow cytometry (FACScalibur, Becton-Dickinson, Franklin Lakes, NJ, USA) with excitation and emission wavelengths of 488 nmand 530 nm, respectively.

3. Results

3.1. Physical properties of the synthesized water-soluble GeNP

GeNP was fabricated by a reduction method. Transmission electron microscopic analysis of the fabricated GeNP revealed an average particle size of 4.2 ± 1.2 nm and is lower than the relatively large excitation Bohr radius (11.2 nm, data not shown). The GeNP exhibits blue photoluminescence at 450 nm with a full width at half maximum of 100 nm (Fig. 1A). Using hydride reducing agents in these experiments produce hydrogen-terminated GeNP surfaces (Warner and Tilley, 2006), which can be treated with compounds containing C=C bond and H_2PtCl_6 catalyst to produce a variety of surface types. We modified the GeNPs with allyamine. Fourier IR spectrum analysis detected the allyamine groups on the surface of GeNP (Fig. 1B). The transmittance at 2900 and 3500 cm^{-1} attribute to asymmetric and symmetric vibration of C–NH_2 and C–CH_2 bonds of the allyamine while the peak at 1661 cm^{-1} is attributed to the allyamine and clearly indicative of its attachment to GeNP. The modified nanoparticles are designated as water-soluble GeNP (wsGeNP) for the following studies.

Physical properties associate with subsequent experiments were also examined prior to applying the wsGeNP to biological samples. The fluorescence intensity of wsGeNP is stable as incubated at different temperatures (4, 37 or 50 °C) for at least 48 h (Fig. 1C). Similar characteristic was also observed when wsGeNP was incubated at different pH (3–10) at 37 °C for 24 h (Fig. 1D). These results indicate that the wsGeNP was stable enough under various experimental conditions for subsequent studies. The emission of blue fluorescence was diminished when wsGeNP was treated with 8 N nitric acid at 65 °C for 12 h, indicating the collapse of the particle structure (Fig. 1E). This condition was then used to estimate the Ge content for the fabricated particles by inductively coupled plasma-mass spectrometry.

3.2. Cytotoxic effect of ws GeNP

Cytoxicity of the wsGeNP was examined. Ge content in the solution was determined by ICP-MS before adding to cells. Cell viability was initially measured by MTT assay. Cells were treated with various concentrations of wsGeNP for 24 h and survival fractions were determined. As shown in Fig. 2A, cell viability declined at as low as 1 μM of wsGeNP and toxicity observed at higher than 3 μM. Since

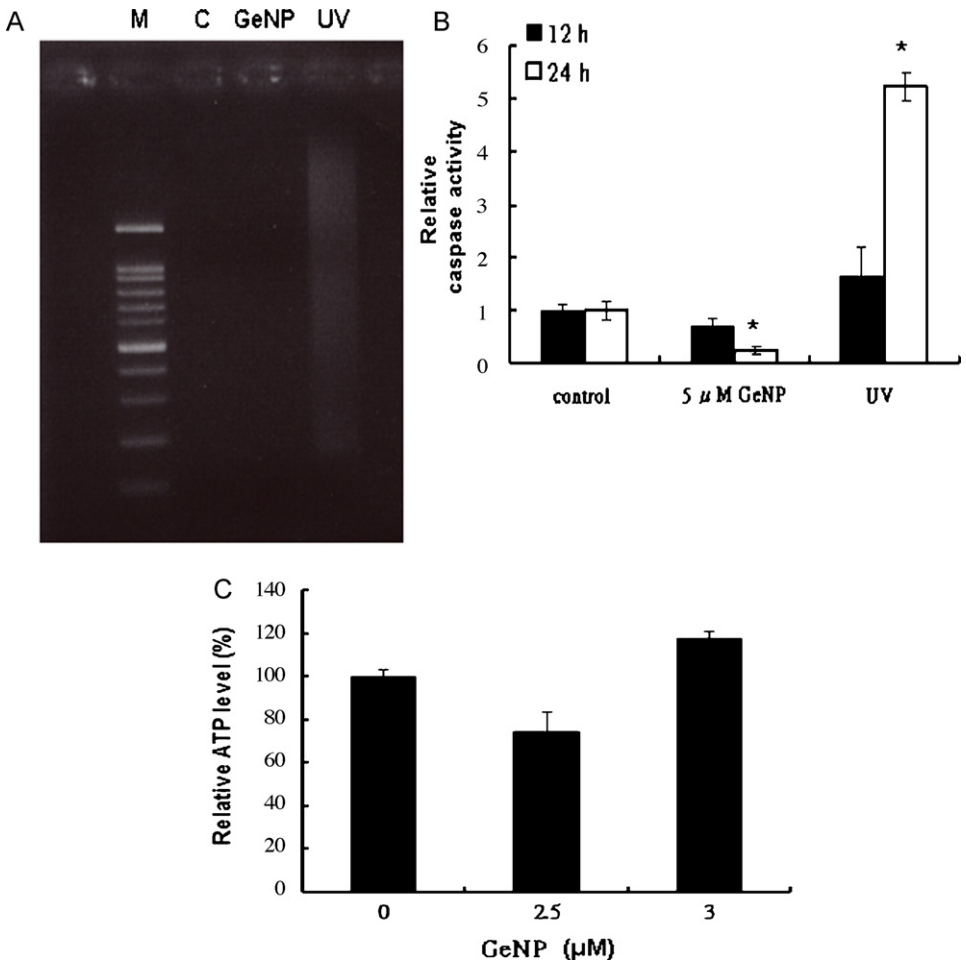

Fig. 3. Characterization of wsGeNP-induced cell death. Cells were treated with 5 μM wsGeNP for 24 h or irradiation with 25 J/m^2 UV. The levels of DNA fragmentation (A) and caspase3 activity (B) were analyzed. Cells were harvested 24 h (A) or 12 and 24 h (B) after UV-irradiation. ATP level was determined in cells after 24 h wsGeNP treatment (C). Each value represents a mean ± standard deviation of three samples. *Significant difference ($p < 0.05$).

germanium oxide (GeO_2) solution did not cause significant cytotoxicity even at millimolar level (Chiu et al., 2002), we speculated that the toxic effect came from the chemical reagent used in producing the wsGeNP. The same procedures for wsGeNP synthesis were then performed in the absence of germanium chloride. The resulting solution was used to examine the cytotoxic effect. No toxic effect was observed for the solvent (data not shown). Chlorogenic survival assay was used to confirm the decrease viability observed in MTT assay. As shown in Fig. 2B, cell viability dropped dose-dependently with the increase of wsGeNP concentration. The results indicate that GeNP synthesized in this work possesses toxic effect.

Since we have shown previous that GeO_2 blocked cell cycle progression (Chiu et al., 2002), we examined whether the wsGeNP processes similar characteristic. Flow cytometric analysis was conducted to examine the cell distribution profile. After treating with various concentrations of wsGeNP for 24 h, cell cycle profile remained similar among the treatments (Fig. 2C). No significant cell cycle arrest could be observed.

3.3. wsGeNP caused necrotic cell death

Cytometric analysis did not detect cells in sub-G1 fraction (Fig. 2C). This result suggests that GeNP treatment did not lead to apoptotic cell death. To demonstrate this effect, DNA fragmentation assay was conducted. As indicated in Fig. 3A, DNA fragmentation was not noted in wsGeNP-treated cells. However, cells after UV irradiation were subjected to apoptotic death and have fragmented DNA. Since caspase 3 is the effector enzyme that causes cell apoptosis, we examine its activity after treatment. Fig. 3B shows that caspase 3 activity did not increase but decreased after wsGeNP treatment. The result was again contrary to that of UV-irradiated cells which showed an increase in caspase activity. For apoptotic cells, ATP level remains unchanged within a period of time (Zamaraeva et al., 2005). However, wsGeNP treatment altered cellular ATP level despite that no correlation could be established between the ATP level and doses of wsGeNP (Fig. 3C). These results suggest that GeNP causes necrotic cell death in CHO K1 cells.

3.4. Necrostatin 1 rescues cells from necrotic death

Cell necrosis leads to the loss of membrane integrity and allows PI to diffuse into cells. Relative cell viability can thus be analyzed via the level of PI uptake. After treating cells for 24 h, wsGeNP caused a dose-dependent loss of cell membrane integrity (Fig. 4A). Comparable to the MTT assay, a significant increase of cellular PI uptake was noted when 2.5 μM wsGeNP was administered to cells. A time-course study was subsequently conducted and the result shows that increase in PI uptake occurs within 12–24 h after adding 5 μM wsGeNP (Fig. 4B). PI exclusion assay is thus used to estimate cell damage in subsequent studies.

Necrotic cell death is currently recognized to proceed in a programmed manner. Interruption of the signal transduction can reduce cell damage. An inhibitor, necrostatin-1 (Nec-1), can attenuate the occurrence of necrotic cell death (Degterev et al., 2005).

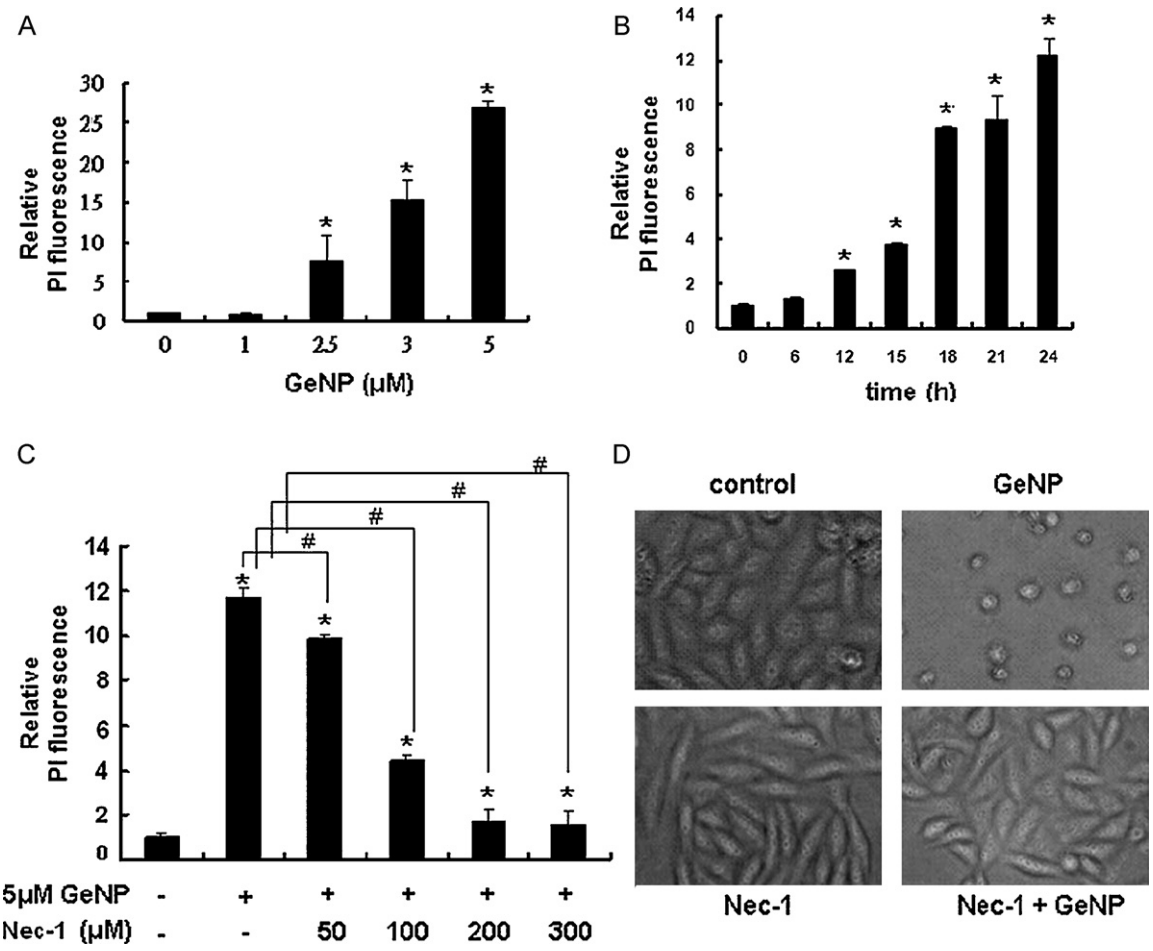

Fig. 4. wsGeNP causes necrotic cell death and can be rescued by Nec-1. Cell membrane integrity was estimated with the PI exclusion assay with: (A) cells treated with various concentrations of wsGeNP for 24 h; (B) cells treated with 5 μM wsGeNP for various time intervals; (C) cells treated with 5 μM wsGeNP in the presence of various concentrations of Nec-1 for 24 h. Each value represents a mean ± standard deviation of three samples. *Significant difference ($p < 0.05$). #Significant ($p < 0.05$) difference between the paired groups. (D) Morphology of cells received 5 μM wsGeNP and/or 300 μM Nec-1 was recorded. Magnitude of amplification: 400×.

Nec-1 was therefore used to verify the damaging effect. As shown in Fig. 4C, Nec-1 is able to reduce the wsGeNP-induced cytotoxic effect. The rescue of cell damage can be correlated with the morphological changes of cells. Cells treated with wsGeNP have a round-up morphology. With the addition of Nec-1, cell morphology returned to that of untreated cells (Fig. 4D). These results demonstrate further that wsGeNP causes necrotic cell death and the damage can be blocked by Nec-1.

3.5. Signaling factors involved in the cell damage induced by wsGeNP

Since wsGeNP-treated cells subjected to necrotic cell death, signaling factors involved in the damage were investigated. Intracellular calcium concentration was examined initially because elevation of calcium content is frequently observed in cells exposed to metal. Cells were treated with 3 or 5 μM wsGeNP for 24 h and calcium content was estimated by flow cytometry. Fig. 5A shows that calcium content increases with the treatment. A time-course study was subsequently conducted and showed that intracellular calcium content increased 12 h after the treatment (Fig. 5B). To analyze whether the elevated calcium content is related to cell damage, intracellular calcium chelator (BAPTA-AM) was added to GeNP-treated cells and reduced the cellular calcium level (Fig. 5C). This reduction correlates to the protective role of the chelator since the level of PI uptake dropped with the increments of BAPTA-AM (Fig. 5D). BAPTA-AM did not recover the cell morphology of the wsGeNP-treated cells since the calcium chelator itself altered the cell morphology (Fig. 5D). This result suggests that wsGeNP stimulates the release of intracellular calcium that leads to cell damage.

Reactive oxygen species (ROS) can be produced by metal challenge and stimulated by elevating cellular calcium content. We therefore estimate the ROS level after wsGeNP treatment. As shown in Fig. 6A, a dose-dependent increase of ROS level was observed in cells after 24 h of GeNP exposure. Time-course study shows that the increase of ROS occurred at 15 h after GeNP treatment (Fig. 6B). An antioxidant, N-acetyl cysteine (NAC), was added to examine whether the ROS can be removed and consequently reduces cell damage. Fig. 6C shows that the ROS was effectively diminished by the antioxidant in a dose-dependent manner. Addition of NAC to wsGeNP-treated cells also abrogated cellular PI uptake (Fig. 6D) and recovered cell morphology (Fig. 6E). These results indicate that NAC prevents cells from damages caused by wsGeNP.

Alternation of mitochondrial membrane potential (MMP) can be found in cells subjected to various stresses resulting in cell death through either apoptotic or necrotic pathway. The role of MMP in wsGeNP-induced damage is then investigated. A reduction in MMP was noted in cells treated with more than 3 μM wsGeNP for 24 h (Fig. 7A). Drop in MMP became significant at 21 h in the presence of 3 μM wsGeNP (Fig. 7B). To link the alternation of MMP with cell damage, cyclosporin A (CsA), which inhibits the opening of the mitochondria membrane transition

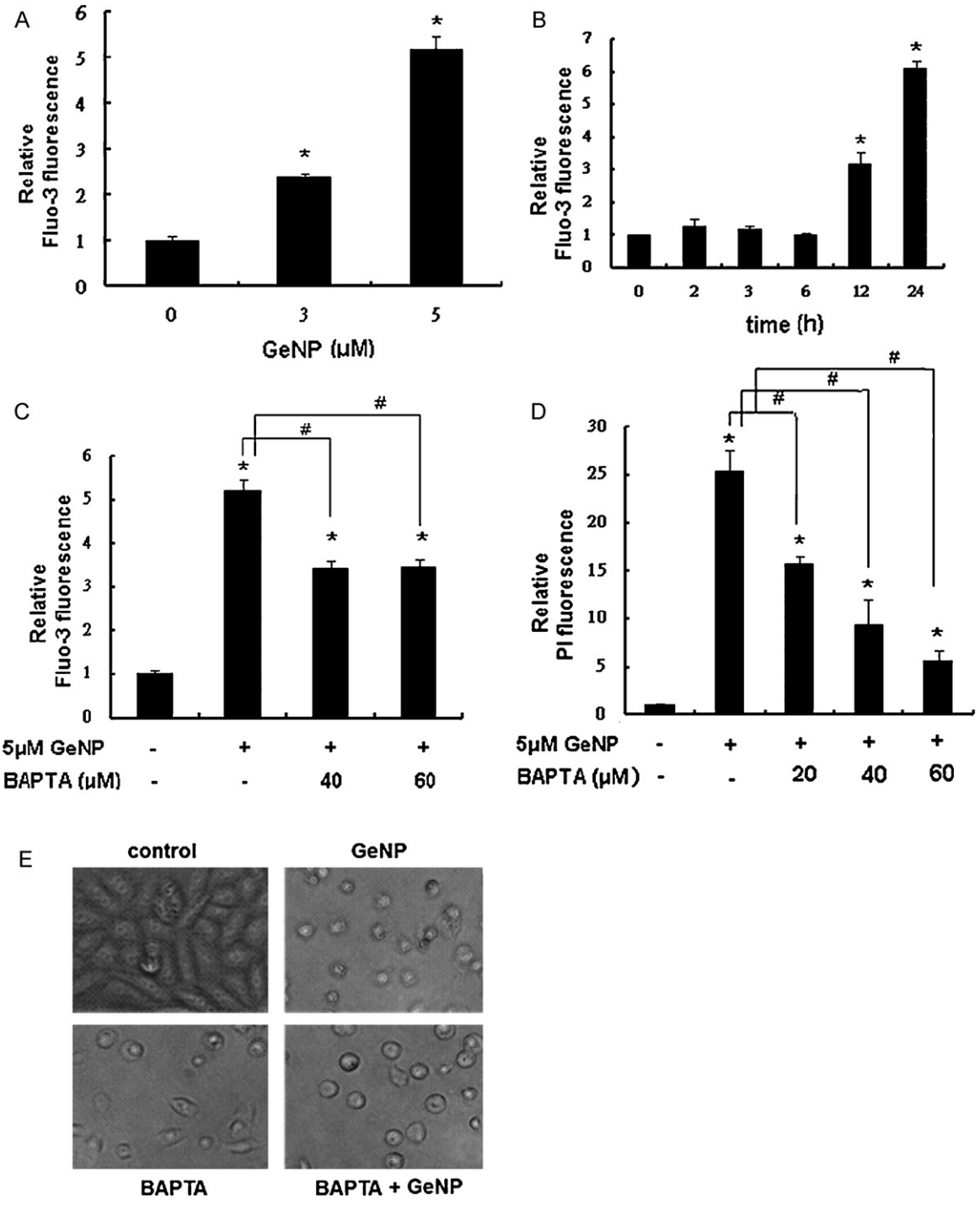

Fig. 5. wsGeNP treatment elevated intracellular Ca^{2+} and caused cell damage. (A) Cells were treated with 3 or 5 μM wsGeNP for 24 h and intracellular Ca^{2+} level was determined. (B) Cells were treated with 5 μM wsGeNP for various time intervals and intracellular Ca^{2+} level was determined. Cells were treated with 5 μM wsGeNP for 24 h in the presence of various concentrations of BAPTA-AM. Intracellular Ca^{2+} (C) or PI uptake (D) level was determined. Each value represents a mean ± standard deviation of three samples. *Significant difference ($p < 0.05$). #Significant ($p < 0.05$) difference between the paired groups. (D) Cell morphology in the presence of 5 μM wsGeNP and/or 60 μM BAPTA-AM was recorded. Magnitude of amplification: 400×.

pore, was used to block the reduction of MMP. Employment of the inhibitor can recover the wsGeNP-induced reduction of MMP (Fig. 7C). Moreover, the blockage of MMP reduction correlated with the level of cell damage since CsA reduced also PI uptake in cells treated with wsGeNP for 24 h (Fig. 7D). The effectiveness of CsA in protecting cell from wsGeNP damage can also be noted by the alternation of cell morphology. With the addition of CsA, the morphology of wsGeNP-treated cells returned to that of untreated cells (Fig. 7E).

3.6. Sequence of the signaling events after GeNP exposure

It is evident from the above results that intracellular calcium, ROS and MMP are involved in the signaling pathway for the wsGeNP-induced cell damage. The alternations of these signaling factors occur respectively at 12, 15 and 21 h, implying a sequence of event occurs from intracellular calcium, ROS to MMP. To demonstrate this sequence, calcium chelator was first applied, then ROS and MMP levels were determined. Fig. 8 shows that ROS was

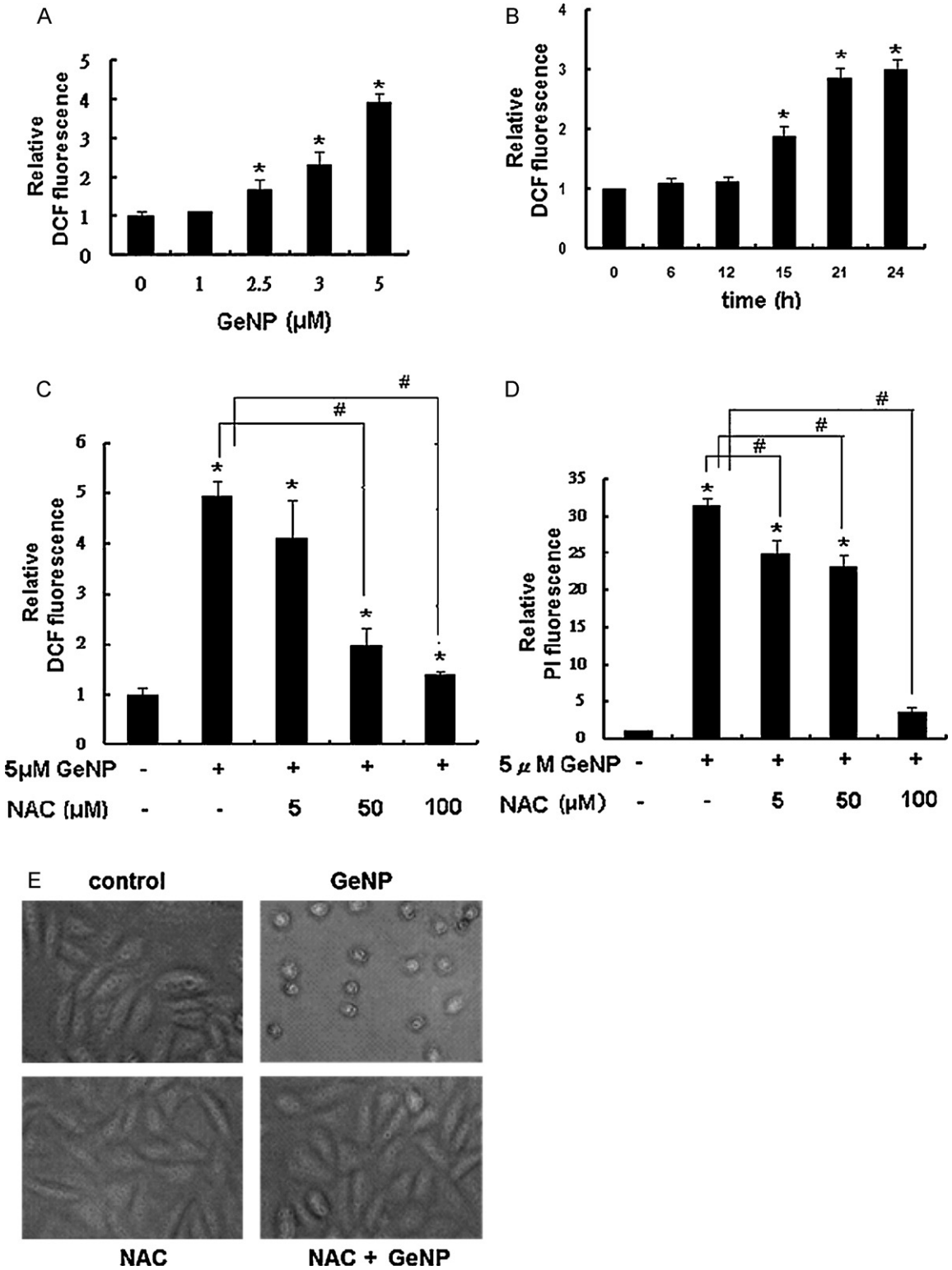

Fig. 6. wsGeNP treatment increased ROS level and caused cell damage. (A) Cells were treated with various concentrations of wsGeNP for 24 h and ROS level was determined. (B) Cells were treated with 5 μM wsGeNP for various time intervals and ROS level was determined. Cells were treated with 5 μM wsGeNP for 24 h in the presence of various concentrations of NAC. ROS (C) or PI uptake (D) level was determined. Each value represents a mean ± standard deviation of three samples. *Significant difference ($p < 0.05$). #Significant ($p < 0.05$) difference between the paired groups. (D) Cell morphology in the presence of 5 μM wsGeNP and/or 100 μM NAC was recorded. Magnitude of amplification: 400×.

reduced (Fig. 8A) while MMP was elevated (Fig. 8B) after adding BAPTA-AM to wsGeNP-treated cells. This result indicates that ROS and MMP are the downstream signals for the increased calcium content. Secondly, NAC was administrated to wsGeNP-treated cells to reduce ROS, then calcium content and MMP were estimated. An elevation in MMP was noted, but the calcium level remained high with the treatment (Fig. 8C and D). This finding shows that ROS is downstream of calcium signaling but upstream of MMP. Thirdly,

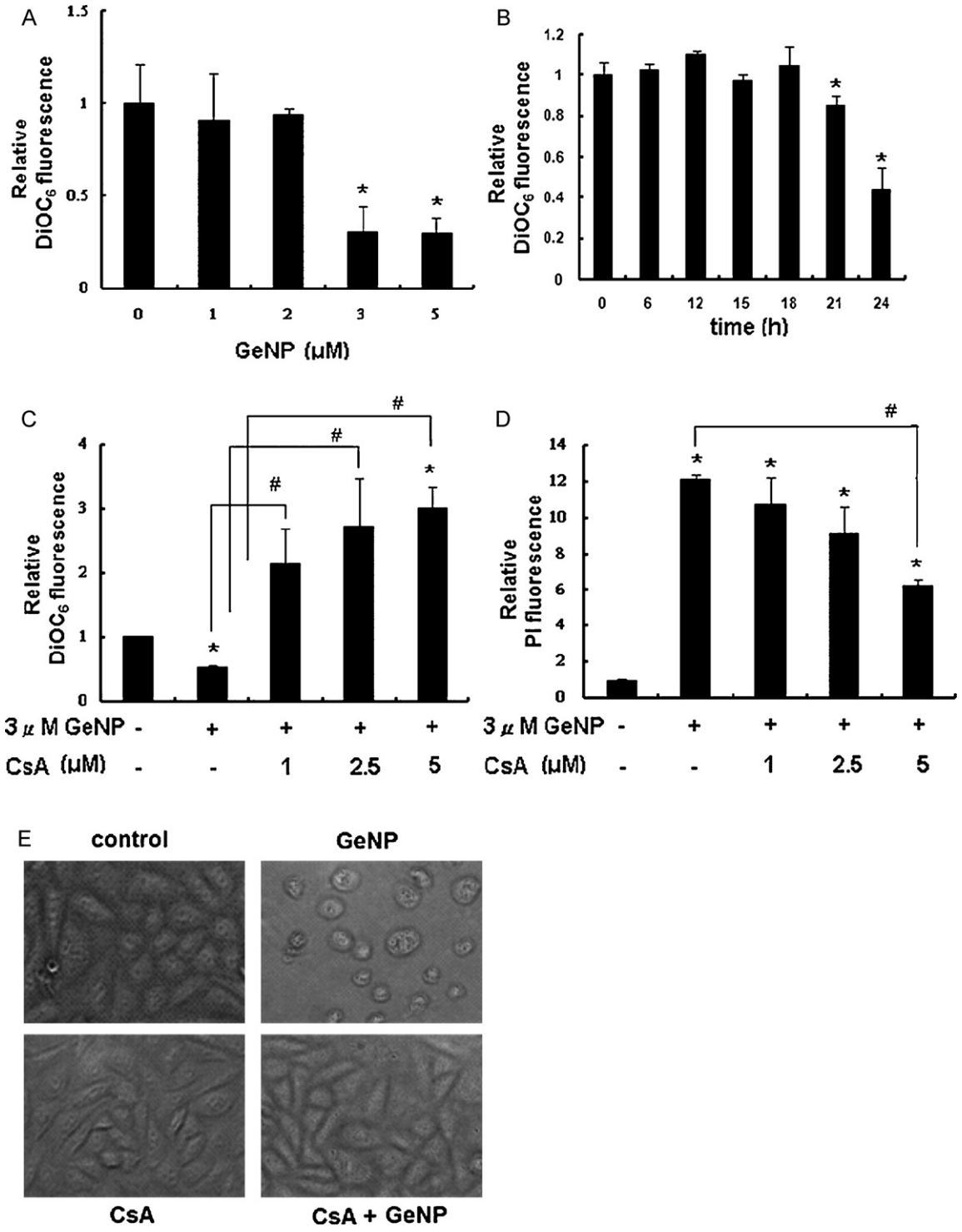

Fig. 7. GeNP treatment reduced MMP level and caused cell damage. (A) Cells were treated with various concentrations of wsGeNP for 24 h and MMP level was determined. (B) Cells were treated with 3 μM wsGeNP for various time intervals and MMP level was determined. Cells were treated with 3 μM wsGeNP for 24 h in the presence of various concentrations of CsA. MMP (C) or PI uptake (D) level was determined. Each value represents a mean ± standard deviation of three samples. *Significant difference ($p < 0.05$). #Significant ($p < 0.05$) difference between the paired groups. (D) Cell morphology in the presence of 3 μM wsGeNP and/or 5 μM CsA was recorded. Magnitude of amplification: 400×.

CsA was given to attenuate the reduction of MMP by wsGeNP. Intracellular calcium (Fig. 8E) and ROS levels (Fig. 8F) were not affected by the addition of CsA, indicating that reduction of MMP derives from an increase in intracellular calcium content and the subsequent augmented ROS level by the wsGeNP treatment. A summary of the signaling pathway of wsGeNP-induced cell death and the chemicals protecting the cells from damages are shown in Fig. 9.

4. Discussion

GeNP can be produced using different approaches. Whether GeNPs fabricated by different methods have similar biological properties remain to be investigated. In this study, we found that GeNP prepared with different methodologies processed dissimilar biological effects. We reported previously that GeNP fabricated by

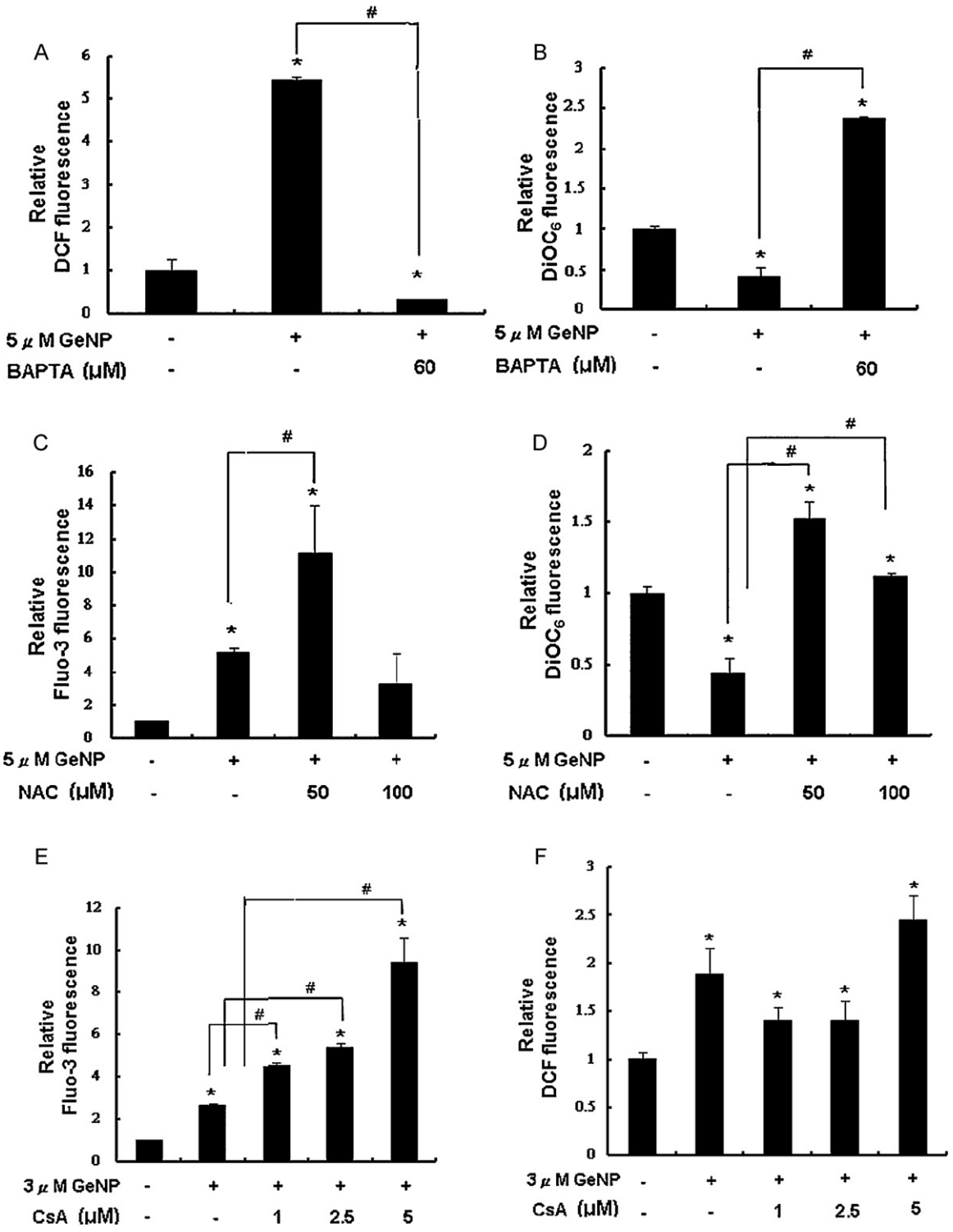

Fig. 8. Determination of the signal sequence for wsGeNP-induced cell damage. (A) ROS and (B) MMP levels were determined in cells treated with 5 μM wsGeNP for 24 h in the presence or absence of 60 μM BAPTA-AM; (C) intracellular Ca^{2+} and (D) MMP levels were determined in cells treated with 5 μM wsGeNP for 24 h in the presence or absence of 50 or 100 μM NAC; (E) intracellular Ca^{2+} and (F) ROS levels were determined in cells treated with 3 μM wsGeNP for 24 h in the presence or absence of 2.5 or 5 μM CsA. Each value represents a mean ± standard deviation of three samples. *Significant difference ($p < 0.05$). #Significant ($p < 0.05$) difference between the paired groups.

vapor condensation method did not exert cytotoxicity to CHO K1 cells (Lin et al., 2009). Additionally, it retards cell cycle progression and enhances radiosensitizing activity of cells. These characteristics are similar to that of GeO_2. However, we found in this study that wsGeNP has toxicity to cells. This finding is unexpected. We examined the physical properties of vapor-condensed GeNP (vpGeNP) and observed that the nanoparticles form aggregates after incubating in water. The vpGeNP can even be decomposed and dissolved in water after standing in room temperature within 2 weeks. The solubilized vpGeNP may show the same property as GeO_2 solution. On the other hand, wsGeNP is physically stable. The fluorescence intensity of wsGeNP remains the same after storing at room temperature for more than 2 months. It can sustain at elevated temperature (50 °C) or acidity (pH 3) for prolonged period

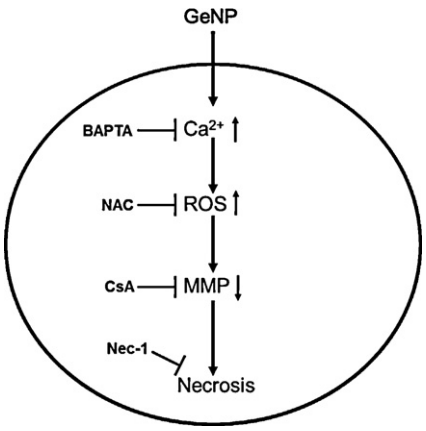

Fig. 9. A schematic illustrating the wsGeNP-induced signaling pathway with chemicals protecting the cells from damages listed.

without affecting the fluorescence intensity. The wsGeNP may be easier to enter and remain intact in cells. These differences in physical properties may attribute to its cytotoxic effect on cells.

Because of the prompt development in nanotechnology, a variety of nanoparticles (NPs) were synthesized. Attempts were made to utilize these NPs for biomedical applications. One of the major concerns about the application is the toxicity to organisms. Cell damaging effects induced by NPs were reported in several studies. Quantum dots with Cd–Se core are known to be toxic to cells due to the release of hazardous metal ions (Medintz et al., 2004). Treating RAW264.7 cells with AgNP resulted in a reduction of cellular GSH content, increased NO production and TNF-α synthesis and subsequent apoptotic cell death (Park et al., 2010). CuNP and MnNP increase oxidative stress via ROS production after entering cells, and lead to cell death (Vanwinkle et al., 2009). These studies indicate that cytotoxicity of the NPs can be derived from the release of the constituents and/or NP-activated signaling pathway(s). Since the dissolved Ge exerts low cell toxicity (Chiu et al., 2002), the damaging effect of wsGeNP comes from the activated signal cascade. Blocking the transduction of the signals rescues cells from necrotic death. This finding indicates that entrance of foreign NPs stimulates various cellular responses. Damages may occur if the cells are not able to manage and modulate the passage of signals.

The degree of cell damage may also be associated with the entrance rate of the NPs. For example, AuNP enters cells rapidly through receptor-mediated endocytosis and activates pro-inflammatory genes such as interleukin I (IL-1), IL-6 and TNF-α (Yen et al., 2009). Owing to higher level of accumulation in cells, AuNP has more significant cytotoxic and immune responses than that induced by AgNP, which entered cells through non-specific endocytosis. Presently, we do not know the exact mechanism for wsGeNP cell entry. We speculate that wsGeNPs enter cells through endocytosis and transiently sequestered in lysosomes. Although the pH of lysosome can be lower than 4, GeNP is stable at pH lower than 3 (Fig. 2). It is unlikely that the wsGeNPs are dissolved in lysosome and the Ge ions leak out to the cytoplasm to produce the toxic effects. Considering that GeO_2 at higher than 20 mM does not exert cellular cytotoxicity after 24 h treatment (Chiu et al., 2002), cell damages should be very limited even if wsGeNP decomposed and releases from lysosomes. Remarkably, damage to the same type of cells can be detected at less than 3 μM of wsGeNP. Because the fluorescence of wsGeNP could not be detected in the cells, cellular localization of the wsGeNP cannot be identified presently. However, intracellular calcium level elevated 12 h after wsGeNP exposure (Fig. 5B). This result implies that the effect was produced after wsGeNP entered cells, but not after the immediate exposure of wsGeNP to cells.

Cells subjected to chemical treatments usually cause a defined type of cell death. However, different types of cell death may occur simultaneously by a treatment. The type of cell death also varies under different conditions; even cells are treated with the same chemical. Cells may subject to apoptotic death under lower chemical concentration, but switches to necrotic death when the dose is high (Majno and Joris, 1995). Studies have indicated that apoptotic and necrotic cell deaths can be regulated by common signaling factors. Alternations in intracellular Ca^{2+}, ROS and MMP are frequently found in either apoptotic or necrotic cell death. Intracellular Ca^{2+} content was reportedly to determine the cell fate (Zong and Thompson, 2006). Moderate elevation of calcium content leads to apoptotic death (McConkey and Orrenius, 1996). However, a great increase of calcium ions results in mitochondrial Ca^{2+} overload and causes necrotic death (Richter and Schlegel, 1993). For wsGeNP-treated cells, a 5-fold increase in intracellular Ca^{2+} content was noted at 5 μM treatment. This raise in Ca^{2+} content is apparently sufficient to initiate the signal for necrosis. Study also showed that ATP level determined the type of cell death. Reduction in ATP content may lead to necrotic cell death (Leist et al., 1997). In our study, we did not observe apoptotic cell death even at high wsGeNP concentration. Although we have demonstrated that wsGeNP caused necrotic cell death, the ATP level did not show a dose-dependent reduction after the treatment. This response is similar to that of peroxynitrite-treated U931 or THP-1 monocytes. This treatment caused necrotic cell death but did not alter cellular ATP level (Cantoni et al., 2005).

The cytotoxic responses of wsGeNP to CHO K1 cells are similar to that of Cd (Yang et al., 2007). Cd-treated cells also rendered necrotic cell death. We showed that the Cd-induced cell damage began with elevation of intracellular Ca^{2+} ions, followed by an increase in ROS level then reduction of MMP; a signaling pathway exactly the same as that of wsGeNP. However, the elevated Ca^{2+} content also stimulates calpain activity in parallel with the ROS increase. Calpain activity was not altered in wsGeNP-treated cells (data not shown). This variation is an example of different chemical treatment stimulates a partially overlapping pathway and leads to similar cell fate.

Report has indicated that different sizes of nanoparticles may produce different cytotoxic effects (Frohlich et al., 2009). For example, treating cells with 1.4 nm AuNP resulted in necrotic cell death. However, the toxicity can be reduced by increasing the particle sizes (Pan et al., 2007). Since the vpGeNP aggregates in water and is not cytotoxic, we speculate that the size of the GeNP may play roles in determining cytotoxicity. Since the size of NP can be modulated by surfactant in the fabrication process (Dung et al., 2009; Natarajan et al., 1996), we increased the concentration of TOAQ to generate wsGeNP with larger sizes (50 and 150 nm diameter in average). A reduction in cytotoxicity (determined by PI exclusion assay) was noted when the larger size wsGeNP was examined. Significant increase of PI uptake was observed after adding 100 μM of the 150 nm wsGeNP for 24 h (data not shown). However, the toxicity is not reduced in a size-dependent manner. Nevertheless, the result suggests that the size of wsGeNP attributes in part the toxicity to cells.

Besides to particle sizes, the cytotoxicity of wsGeNP may vary in different cell types. We have examined the toxicity of wsGeNP in HEK293 cells and found a significant increase in PI uptake when the concentration reached 20 μM. This result indicates a cell specific damaging effect of the wsGeNP. Cell-type specific toxicity has been reported in several studies. ZnO NP produced varied cytotoxic effect to human immune cells; lymphocytes are most resistant while monocytes are most susceptible to the toxicity (Kauzlarich et al., 2004). Cytotoxicity of silica NP also showed a strong dependence on cell type and particle size when human epithelial cells and mouse monocytes were compared (Diaz et al., 2008; Warner and

Tilley, 2006). We used CHO K1 cells in this study such that the Ge effect can be compared with our previous works. Although wsGeNP exerts less toxic effect in human kidney cell (HEK293), the toxicity is still present.

We established in this work the signaling pathway of wsGeNP-induced cell damage. A variety of metallic compounds have reported to transduce cytotoxicity via the Ca^{2+}/ROS/MMP pathway. This pathway may also be common to NP-activated cell damages. Signals through this common pathway cause either apoptotic or necrotic death depending on the cell type and the property of the NP. We show here that wsGeNP causes necrotic cell death and Nec-1 can attenuate NP-induced necrotic cell death. This is the first study to indicate the effectiveness of Nec-1 and thus provides a potential antagonist to counteract the hazard of NP exposure. We have suggested previously that reduction in MMP after chemical treatment may be a prerequisite for Nec-1 to reduce necrotic cell death (Hsu et al., 2009). Since wsGeNP treatment causes MMP reduction and leads to necrotic cell death, Nec-1 is effective in rescuing damaged cells.

In summary, we reported here the toxicological study of wsGeNP. In contract to GeO_2 and vpGeNP, wsGeNP showed high toxicity to cells. It caused cell necrosis through elevating intracellular calcium concentration which results in an increase in ROS level. ROS stimulates the reduction of MMP and leads cells to necrotic death. This damaging effect can be attenuated by adding calcium chelator, ROS scavenger, MPT pore inhibitor or Nec-1.

Acknowledgements

This work was supported by grants NSC95-2627-M-007-006 and NSC96-2627-M-007-006 from the National Science Council, Taiwan, Republic of China. The authors thank Dr. M.F. Tam for critical reading of the manuscript.

References

Alivisatos, P., 2004. The use of nanocrystals in biological detection. Nat. Biotechnol. 22, 47–52.
Aso, H., Suzuki, F., Ebina, T., Ishida, N., 1989. Antiviral activity of carboxyethylgermanium sesquioxide (Ge-132) in mice infected with influenza virus. J. Biol. Response Mod. 8, 180–189.
Bailey, S.G., Raffaelle, R., Emery, K., 2002. Space and terrestrial photovoltaics: synergy and diversity. Prog. Photovoltaics 10, 399–406.
Cantoni, O., Guidarelli, A., Palomba, L., Fiorani, M., 2005. U937 cell necrosis mediated by peroxynitrite is not caused by depletion of ATP and is prevented by arachidonate via an ATP-dependent mechanism. Mol. Pharmacol. 67, 1399–1405.
Chiu, H.W., Kauzlarich, S.M., 2006. Investigation of reaction conditions for optimal germanium nanoparticle production by a simple reduction route. Chem. Mater. 18, 1023–1028.
Chiu, H.W., Kauzlarich, S.M., Sutter, E., 2006. Thermal behavior and film formation from an organogermanium polymer/nanoparticle precursor. Langmuir 22, 5455–5458.
Chiu, S.J., Lee, M.Y., Chen, H.W., Chou, W.G., Lin, L.Y., 2002. Germanium oxide inhibits the transition from G2 to M phase of CHO cells. Chem. Biol. Interact. 141, 211–228.
Degterev, A., Huang, Z., Boyce, M., Li, Y., Jagtap, P., Mizushima, N., Cuny, G.D., Mitchison, T.J., Moskowitz, M.A., Yuan, J., 2005. Chemical inhibitor of nonapoptotic cell death with therapeutic potential for ischemic brain injury. Nat. Chem. Biol. 1, 112–119.
Diaz, B., Sanchez-Espinel, C., Arruebo, M., Faro, J., Miguel, E.d., Magadan, S., Yague, C., Fernandez-Pacheco, R., Ibarra, M., Santamaria, J., Gonzalez-Fernandez, A., 2008. Assessing methods for blood cell cytotoxic responses to inorganic nanoparticles and nanoparticle aggregates. Small 4, 2025–2034.
Dozono, H., Ikeda, K., Onishi, T., 1996. Effectiveness of Ge-132 to relieve pain and smooth home care administration for the terminal cancer patient. Gan To Kagaku Ryoho 23 (Suppl. 3), 291–295.
Dung, T.T.N., Buu, N.Q., Viet Quang, D., Thi Ha, H., Bang, L.A., Hoai Chau, N., Thi Ly, N., Trung, N.V., 2009. Synthesis of nanosilver particles by reverse micelle method and study of their bactericidal properties. J. Phys.: Conf. Ser. 187, 012054.
Fok, E., Shih, M., Meldrum, A., Veinot, J.C., 2004. Preparation of alkyl-surface functionalized germanium quantum dots via thermally initiated hydrogermylation. Chem. Commun., 386–387.
Frohlich, E., Samberger, C., Kueznik, T., Absenger, M., Roblegg, E., Zimmer, A., Pieber, T.R., 2009. Cytotoxicity of nanoparticles independent from oxidative stress. J. Toxicol. Sci. 34, 363–375.
Fukazawa, H., Ohashi, Y., Sekiyama, S., Hoshi, H., Abe, M., Takahashi, M., Sato, T., 1994. Multidisciplinary treatment of head and neck cancer using BCG, OK-432, and GE-132 as biologic response modifiers. Head Neck 16, 30–38.
Hsu, T.S., Yang, P.M., Tsai, J.S., Lin, L.Y., 2009. Attenuation of cadmium-induced necrotic cell death by necrostatin-1: potential necrostatin-1 acting sites. Toxicol. Appl. Pharmacol. 235, 153–162.
Kauzlarich, S.M., Zou, J., Baldwin, R.K., Pettigrew, K.A., 2004. Solution synthesis of ultrastable luminescent siloxane-coated silicon nanoparticles. Nano Lett. 4, 1181–1186.
Kumano, N., Ishikawa, T., Koinumaru, S., Kikumoto, T., Suzuki, S., Nakai, Y., Konno, K., 1985. Antitumor effect of the organogermanium compound Ge-132 on the Lewis lung carcinoma (3LL) in C57BL/6 (B6) mice. Tohoku J. Exp. Med. 146, 97–104.
Lambert, T.N., Andrews, N.L., Gerung, H., Boyle, T.J., Oliver, J.M., Wilson, B.S., Han, S.M., 2007. Water-soluble germanium(0) nanocrystals: cell recognition and near-infrared photothermal conversion properties. Small 3 (4), 691–699.
Leist, M., Single, B., Castoldi, A.F., Kuhnle, S., Nicotera, P., 1997. Intracellular adenosine triphosphate (ATP) concentration: a switch in the decision between apoptosis and necrosis. J. Exp. Med. 185, 1481–1486.
Lin, M.H., Hsu, T.S., Yang, P.M., Tsai, M.Y., Perng, T.P., Lin, L.Y., 2009. Comparison of organic and inorganic germanium compounds in cellular radiosensitivity and preparation of germanium nanoparticles as a radiosensitizer. Int. J. Radiat. Biol. 85, 214–226.
Lu, X., Korgel, B.A., Johnston, K.P., 2005. High yield of germanium nanocrystals synthesized from germanium diiodide in solution. Chem. Mater. 17, 6479–6485.
Majno, G., Joris, I., 1995. Apoptosis, oncosis, and necrosis. An overview of cell death. Am. J. Pathol. 146, 3–15.
McConkey, D.J., Orrenius, S., 1996. The role of calcium in the regulation of apoptosis. J. Leukoc. Biol. 59, 775–783.
Medintz, I.L., Trammell, S.A., Mattoussi, H., Mauro, J.M., 2004. Reversible modulation of quantum dot photoluminescence using a protein-bound photochromic fluorescence resonance energy transfer acceptor. J. Am. Chem. Soc. 126, 30–31.
Michalet, X., Pinaud, F.F., Bentolila, L.A., Tsay, J.M., Doose, S., Li, J.J., Sundaresan, G., Wu, A.M., Gambhir, S.S., Weiss, S., 2005. Quantum dots for live cells, *in vivo* imaging, and diagnostics. Science 307, 538–544.
Natarajan, U., Handique, K., Mehra, A., Bellare, J.R., Khilar, K.C., 1996. Ultrafine metal particle formation in reverse micellar systems: effects of intermicellar exchange on the formation of particles. Langmuir 12, 2670–2678.
Ngiam, S.-T., Jensen, K.F., Kolenbrander, K.D., 1994. Synthesis of Ge nanocrystals embedded in a Si host matrix. J. Appl. Phys. 76, 8201.
Pan, Y., Neuss, S., Leifert, A., Fischler, M., Wen, F., Simon, U., Schmid, G., Brandau, W., Jahnen-Dechent, W., 2007. Size-dependent cytotoxicity of gold nanoparticles. Small 3, 1941–1949.
Park, E.J., Yi, J., Kim, Y., Choi, K., Park, K., 2010. Silver nanoparticles induce cytotoxicity by a Trojan-horse type mechanism. Toxicol. In Vitro 24, 872–878.
Riabinina, D., Durand, C., Chaker, M., Rowell, N., Rosei, F., 2006. A novel approach to the synthesis of photoluminescent germanium nanoparticles by reactive laser ablation. Nanotechnology 17, 2152–2155.
Richter, C., Schlegel, J., 1993. Mitochondrial calcium release induced by prooxidants. Toxicol. Lett. 67, 119–127.
Rieke, G.H., 2007. Infrared detector arrays for astronomy. Annu. Rev. Astron. Astr. 45, 77–115.
Singh, A.K., Kumar, V., Kawazoe, Y., 2005. Design of a very thin direct-band-gap semiconductor nanotube of germanium with metal encapsulation. Phys. Rev. 71, 75312.
Thiele, U.K., 2001. The current status of catalysis and catalyst development for the industrial process of poly(ethylene terephthalate) polycondensation. Int. J. Polym. Mater. 50, 387–394.
Vanwinkle, B.A., de Mesy Bentley, K.L., Malecki, J.M., Gunter, K.K., Evans, I.M., Elder, A., Finkelstein, J.N., Oberdorster, G., Gunter, 2009. Nanoparticle (NP) uptake by type I alveolar epithelial cells and their oxidant stress response. Nanotoxicology 3, 307–318.
Warner, J.H., Tilley, R.D., 2006. Synthesis of photoluminescence water-soluble germanium nanocrystals. Nanotechnology 17, 3745–3749.
Washio, K., 2003. SiGe HBT and BiCMOS technologies for optical transmission and wireless communication systems. IEEE Trans. Electron. Dev. 50, 656–668.
Xie, P., Hu, Y., Fang, Y., Huang, J., Lieber, C.M., 2009. Diameter-dependent dopant location in silicon and germanium nanowires. Proc. Natl. Acad. Sci. U.S.A. 106, 15254–15258.
Yang, P.M., Chen, H.C., Tsai, J.S., Lin, L.Y., 2007. Cadmium induces Ca2+-dependent necrotic cell death through calpain-triggered mitochondrial depolarization and reactive oxygen species-mediated inhibition of nuclear factor-kappaB activity. Chem. Res. Toxicol. 20, 406–415.
Yen, H.J., Hsu, S.H., Tsai, C.L., 2009. Cytotoxicity and immunological response of gold and silver nanoparticles of different sizes. Small 5, 1553–1561.
Zamaraeva, M.V., Sabirov, R.Z., Maeno, E., Ando-Akatsuka, Y., Bessonova, S.V., Okada, Y., 2005. Cells die with increased cytosolic ATP during apoptosis: a bioluminescence study with intracellular luciferase. Cell Death Differ. 12, 1390–1397.
Zhou, Z., Brus, L., Friesner, R., 2003. Electronic structure and luminescence of 1.1- and 1.4-nm silicon nanocrystals: oxide shell versus hydrogen passivation. Nano Lett. 3, 163.
Zong, W.X., Thompson, C.B., 2006. Necrotic death as a cell fate. Genes Dev. 20, 1–15.